

# Real-Time Intelligent Audio and Object Detection for Robotics Systems

By

Raghav Atal

Steve Barry

Venku Buragadda

Daniel Dobrzynski

J. Nick Gallagher

Marcus Himelhoch

Brian Kremzier

Kai Li

Abigail L. Matthews

Christopher B. Olen

Sasha Roberts

Audrey Salerno

Rashmi Ranjan Samal

Scott Shepard

Kevin Stutenberg

L. Victoria Waring

Advisor: Yuri Balasanov, Ph.D.

A capstone project submitted to the University of Chicago in partial fulfillment of the  
requirements for the degree of Master of Science in Analytics

Chicago, Illinois

June 2020

The Capstone Project Committee for

Raghav Atal  
Steve Barry  
Venku Buragadda  
Daniel Dobrzynski  
J. Nick Gallagher  
Marcus Himelhoch  
Brian Kremzier  
Kai Li  
Abigail L. Matthews  
Christopher B. Olen  
Sasha Roberts  
Audrey Salerno  
Rashmi Ranjan Samal  
Scott Shepard  
Kevin Stutenberg  
L. Victoria Waring

certifies that this is the approved version of the following capstone project report:

*Real-Time Intelligent Audio and Object Detection for Robotics Systems.*

---

**Project Title**

---

**Project Supervisor**

---

**Program Director**

## **Abstract**

We present three separate object detection and audio classification schemes for robotics applications using the Raspberry Pi 4. Each application builds on advancements within the fields of object detection and audio classification to-date and takes advantage of the increased computational power of the Raspberry Pi 4. We ultimately test each application against a predetermined set of robotics tasks in the form of a scavenger hunt. Our findings suggest: the Raspberry Pi 4 can effectively manage five threads in parallel but the optimal number of threads may depend on the tasks performed on each; deep learning methods out-perform probabilistic approaches to audio classification; crucial efficiency gains can be obtained from using portable USB accelerators and edge computing-optimized models; object detection models for robotics tasks in particular must be trained on a wide variety of data given the high degree of training bias.

Keywords: Deep Learning, Object Detection, Audio Detection, Robotics, Parallel Processing, Multithreading, Transfer Learning

## **Table of Contents**

Introduction.....	05
Literature Review.....	07
Methodology.....	19
Findings.....	46
Summary and Conclusions.....	51
References.....	54

## **Introduction**

The Raspberry Pi is one of the latest developments in the evolution of mobile computing technologies over the past few decades. Spurred on by ARM, a British hardware designer whose products were featured in approximately 95% of mobile phones by 2005, the first Raspberry Pi was made available to the public in 2012 (Dennis, 2015).

Concurrently, the growing availability of compute power coupled with deep neural networks has brought on the rise of deep learning. And with this increase in model complexity and computational power, deep learning practitioners have been able to address increasingly complex problems. Deep learning has proved consequential in robotics applications (Goodfellow, Bengio, & Courville, 2016), and indeed, the deep learning revolution has coincided with explosive growth within the robotics industry (Mordor Intelligence, 2019).

This research seeks to explore the capabilities of deep learning algorithms for automation tasks using relatively inexpensive mobile computing equipment such as the Raspberry Pi. Specifically, we hope to determine the most effective deep learning applications for object detection and audio classification on the Raspberry Pi and its compatible hardware interfaces<sup>1</sup>. In doing so, we hope to contribute to the growing numbers of commercial products available for home and light-industry automation (Dennis, 2015).

The fields of object detection, audio classification, and robotics are broad, but many such tasks are performed on state-of-the-art platforms. Our research focuses on applying recent object detection and audio classification advancements to the more restrictive environment of the

---

<sup>1</sup> For this project, we will be relying on Dexter Industries' GoPiGo3 board, which communicates with the Raspberry Pi 4 over an SPI interface. More information about the GoPiGo robot can be found in the Methodology section.

Raspberry Pi. In doing so, we hope to train our robot to intelligently classify 12 classes of household objects, four traffic cones of differing colors, and 10 classes of audio samples.

We will begin with a brief review of the latest advancements in image recognition and audio classification. We hope to take advantage of insights from these domains to propose the most effective models for our Raspberry Pi. We will then detail the discrete robotics tasks in the form of a scavenger hunt challenge toward which we will apply various image recognition, audio classification, and multithreading methodologies. Said tasks will ultimately inform the steps we take to train our models. Finally, we will review the performance of our various methodologies, provide the appropriate conclusions, and suggest directions for future research.

## Literature Review

### **Advancements in Object Detection**

The past two decades have seen a revolution in computer vision, largely driven by the evolution of the Convolutional Neural Network (CNN). Beginning with early architectures such as Yann LeCun's *LeNet-5* in 1998, researchers in computer vision have taken advantage of increasing quantities of labeled image data, growing computational power, and deeper network architectures to vastly reduce the image classification error rates in competitions such as the ILSVRC ImageNet Challenge. More recently, the winner of the 2015 ImageNet challenge was the Residual Network (or *ResNet*): a 152-layer deep CNN that uses residual learning to significantly speed up training (Gerón, 2017).

Object detection takes image recognition a step further by introducing the challenge of localization: given the existence of one or more target objects within an image, how to simultaneously identify the class and location of one or more objects in an image? Early approaches use a sliding-window approach where a classifier is passed over distinct regions of an image, accepting only the inferences with the highest confidence scores to determine image location (Dalal & Triggs 2006; Felzenszwalb et al., 2010). Nonetheless, such approaches are slow on inference, as they require multiple, separate inferences prior to object detection.

#### *You Only Look Once (YOLO)*

First developed in 2015, the first iteration of YOLO (YOLOv1) reframes object detection as a single regression problem by simultaneously predicting the classes and bounding boxes of target images (Redmon et al., 2015). In doing so, it substantially decreases inference time compared to many of its predecessors while maintaining a relatively high degree of accuracy.

During inference, YOLO divides a given image into an  $S \times S$  grid and then predicts  $B$  bounding boxes with center coordinates  $(x, y)$  located in each of the  $S \times S$  grid cells, along with each bounding boxes' height and width. Also, for each grid cell, it provides a confidence score for each of the  $C$  possible object classes. Thus, for each inference, YOLOv1 outputs an  $S \times S \times (B * 5 + C)$ -dimensional tensor. Ultimately, inferences are made by calculating the joint probability of a bounding box containing an object and the grid cell in which the bounding box is centered containing an object of a certain class. Only predictions above a certain threshold are retained (Redmon et al., 2015).

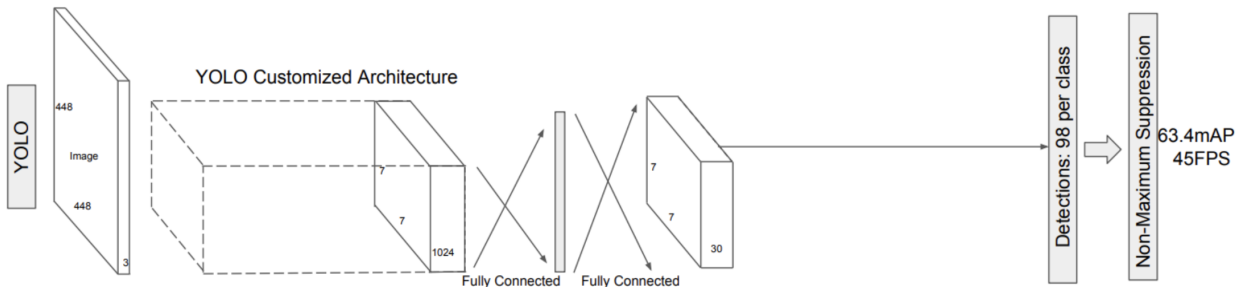


**Figure 1: Model structure of YOLOv1** (Liu et al., 2016)

In the likely event that multiple bounding boxes detect the same object, YOLOv1 uses a technique called Non-Maximal Suppression (NMS), which removes certain duplicative bounding boxes depending on a given bounding box's probability and the extent to which it overlaps with other bounding boxes (Redmon et al., 2015).

Version three of YOLO (YOLOv3) realizes additional performance and efficiency gains. Most notably, this model architecture provides an improved base image classifier in DarkNet-53 and includes multi-scale predictions similar to the Single Shot MultiBox Detector (Redmon et al., 2018). Darknet-53 is primarily composed of  $3 \times 3$  and  $1 \times 1$  filters with skip connections similar to the residual units in ResNet. Darknet-53 also has fewer *billion floating point operations*

(BFLOP) than ResNet-152 but achieves the same classification accuracy in half the time. Unlike many object detectors, YOLOv3 does not use a softmax activation function; instead, it uses individual logistic classifiers to determine the likelihood that an object belongs to a given label versus all other labels. This innovation leads to additional speed improvements. Indeed, YOLOv3 performs inference three times faster than its predecessor with comparable accuracy (Redmon et al., 2018). Finally, YOLOv3’s Feature Pyramid Network (FPN) makes it more adept at detecting small objects vis-a-vis MobileNetV1 SSD, discussed next (Hui, 2018).

#### *The Single Shot MultiBox Detector (SSD)*

The Single Shot MultiBox Detector (SSD) is an additional approach to object detection proposed by Liu et al. (2016). Similar to YOLOv1, SSD can detect multiple objects in a single image by separating the input space into a set of default bounding boxes of various sizes and aspect ratios. One major contribution of SSD is that it predicts object classes and bounding box locations using feature maps of varying scales from different layers throughout the network. Thus, for each of the bounding boxes corresponding to each grid location for each feature map generated by the network, we output confidence scores for all possible object classes in addition to four bounding box offset predictions (one for each edge of the box). The result of these contributions is an 11% increase in mean average precision (mAP) over YOLOv1 and an

increase in speed of 14 frames per second (FPS) over YOLOv1 when using VGG-16 as the base image classifier.

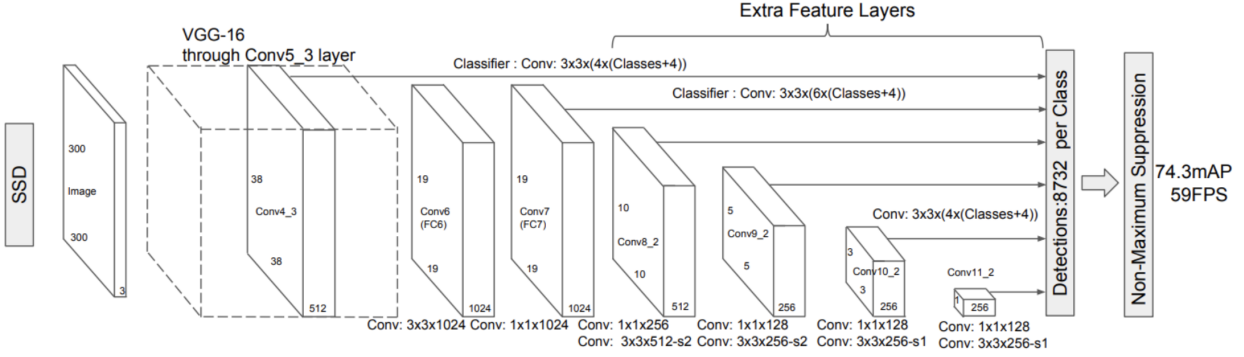


**Figure 2: Model structure of SSD** (Liu et al., 2016)

SSDs can be customized to use different base image classification models for feature extraction. MobileNet SSDs, which use either MobileNet version one (MobileNetV1) or MobileNet version two (MobileNetV2) as their base image classifier, are specialized for mobile and embedded computer vision applications. MobileNetV1 (Howard, et al., 2017) offers an alternative to expensive, traditional convolutions that filter and combine inputs into a new set of outputs all in one step. The so-called *depthwise separable convolutions* factorize the traditional convolutional layer into two component layers: a depthwise convolution to apply a single filter per input channel and a  $1 \times 1$  pointwise convolution to create a linear combination of the depthwise convolution output. This factorization drastically reduces the number of computations required to perform the convolution. The resulting MobileNetV1 model experienced a loss of only 1.1% in top-1 accuracy on ImageNet data compared to similar models using traditional convolutional layers but used seven times fewer parameters.

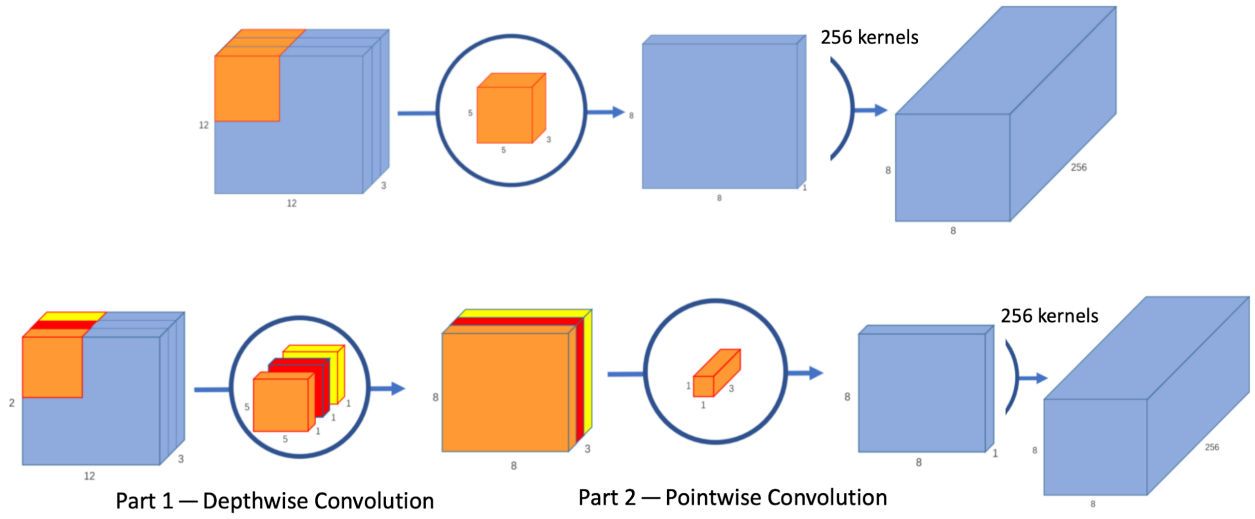


**Figure 3: Depthwise separable convolution.** Top: Depthwise Convolution. Bottom: Pointwise Convolution (Wang, 2018)

Howard, et al. (2019) further improved upon MobleNetV1 with MobileNetV2. They introduce a novel layer module: an *inverted residual with linear bottleneck*. This adds linear bottlenecks between pairs of depthwise separable convolutions and skipped connections between the bottlenecks. The bottlenecks aim to encode the intermediate inputs and outputs, while the intermediate depthwise separable convolutions capture image features.

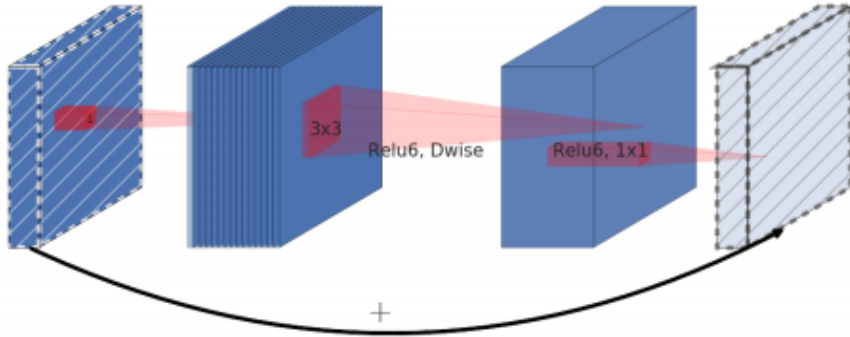


**Figure 4: Inverted residual with linear bottleneck.** Thickness in the figure denotes a relative number of channels. The hashed lines indicate bottlenecks, which are connected together (Howard, et al., 2019).

MobileNetV2 yields a top-1 classification accuracy of 72% on ImageNet data, outperforming MobileNetV1 by 1.4% with a 48% increase in efficiency. MobileNetV2 is further scalable with additional parameters to increase network width and resolution. Scalable networks are discussed in more detail in the next section.

## **Advancements Audio Detection**

The past few decades have seen the advent of various probabilistic and machine learning approaches to audio classification problems. More recently, with the evolution of CNNs, approaches that have been proposed for image recognition have also achieved success within the audio classification domain.

### *Digital Representations of Audio Signals*

When analog audio signals are captured as digital audio signals, they are represented as time series of sampled amplitudes with a known sampling rate. In order to properly analyze and recognize audio signals using learning algorithms, we need a way to also understand the frequency composition. A common method of representing changes in both amplitude and frequency of an audio signal is through a three-dimensional estimate of the *power spectral density* (PSD). Boashash (2016) describes how the PSD distributes the amplitude or power into the frequency components that make up the audio signal. The PSD estimate is generated from the squared magnitude of the windowed *Fast Fourier Transform* (FFT) of the audio signal. The FFT is a discrete Fourier transform of the audio signal used to convert the amplitude from the time domain into the frequency domain. A windowed FFT is also known as a *Short-Term Fourier Transform* (STFT), where the windowing allows the spectrum to be localized in time but results in some blurring of the spectrum across frequencies due to uncertainty relationships in the

frequency resolution. Therefore, the window length of the STFT needs to be tuned to optimize the trade-off between time resolution and frequency resolution.

### *Non-Linear Transformations and Condensed Representations of Audio Signals*

For speech recognition problems, it is common to transform the initial linear frequency scale to better emphasize frequencies that are important to human hearing. A common scaling method is known as the *mel scale*, which is linear below 1 kHz and logarithmic above 1 kHz. This scale is designed to better represent the human-perception of audio signals, where changes in frequency are represented in equal-pitch increments (Boashash, 2016).

*Mel-frequency cepstral coefficients* (MFCC) are condensed representations of the original time domain of an audio signal and have been popular in the speech recognition domain. MFCCs are obtained by mapping the PSD estimate of the audio signal onto the *mel scale*, taking the log of the resulting powers, and applying a discrete cosine transformation to transform back to the time domain (Gales & Young, 2008). Comparing various encoding schemes when applied to speech, Davis and Mermelstein (1980) find that MFCCs are significantly better than comparable methods at suppressing insignificant spectral variation at higher frequencies. Furthermore, MFCCs are particularly adept at providing compact representations of the original time domain, often capturing most of the relevant information in as few as six cepstral coefficients.

### *Image Representations of Audio Signals*

Audio signals can also be represented as spectrograms images. A spectrogram is a two-dimensional representation of the power spectral density of the audio signal, with time on the *x*-axis, frequency on the *y*-axis, and the amplitude of the signal at a given time and frequency represented by the color intensity (with light colors often indicating the higher amplitudes).

Spectrograms can be further transformed into *mel spectrograms* by converting the linear frequency scale to a *mel scale*.

### *Using Image Classification Models for Audio Classification*

The ability to represent audio signals as spectrograms allows us to apply image classification approaches such as CNNs to the problem of audio classification. As with many image classification tasks, the process of training a CNN for audio classification tasks can be aided by starting with a pre-trained CNN and applying transfer learning. We will review a variety of families of scalable CNNs that are pre-trained on large, multi-class, image datasets such as ImageNet.<sup>2</sup>

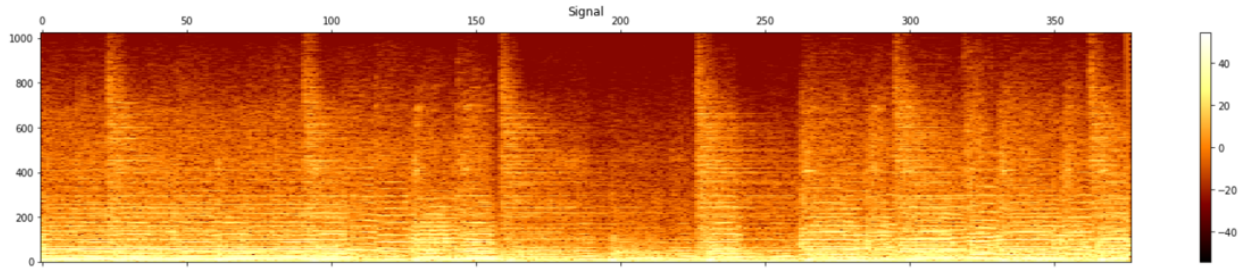


**Figure 5: Spectrogram image**

### *Scalable Convolutional Neural Networks*

A common way to increase the accuracy of a CNN is to increase the depth, width, or input resolution of the network – a technique known as scaling. Typically, only one dimension is scaled, and the most common dimension to scale is the depth. As a network is scaled, accuracy gains come at the cost of increasing resource needs, so scalable CNN families offer multiple size variations from which to choose based on the requirements of the application.

---

<sup>2</sup> Additional details on ImageNet can be found in the *Training Data* subsection of *Methodology*.

In 2019, researchers at Google (Tan & Le, 2019) identified a new method of uniformly scaling a CNN’s width, depth, and input resolution dimensions by a fixed set of scaling coefficients – a technique known as *compound scaling* – resulting in better accuracy and efficiency. Figure 5 below illustrates the differences between single-dimension scaling and compound scaling. Compared to traditional scaling methods, compound scaling results in a 0.7% increase in accuracy for ResNet and a 1.4% increase in accuracy for MobileNet. We discuss these two networks in further detail below.

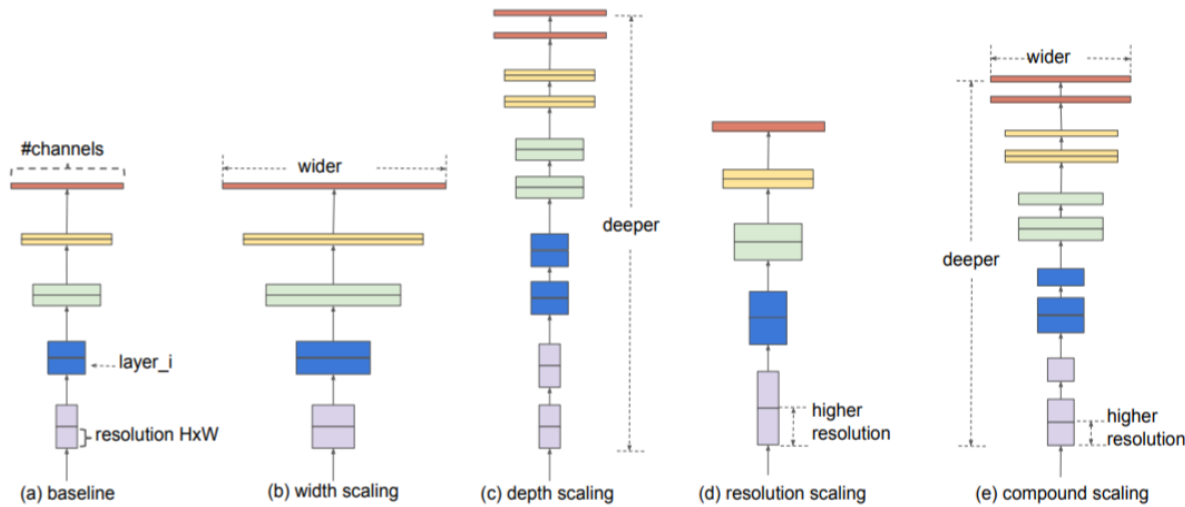


**Figure 6: Model Scaling.** (a) is a base network; (b)-(d) demonstrate conventional scaling along the width (b), depth (c), and resolution (d) dimensions; (e) demonstrates compound scaling using a fixed scaling ratio (Tan & Le, 2019).

### ResNet

ResNet is a CNN developed to address the *degradation problem*. Degradation occurs when, as the complexity of the model increases, the training error increases for reasons other than overfitting. Strategies such as Xavier initialization and batch normalization can prevent overfitting, but additional learning difficulties may persist, resulting in worse performance than shallower networks (Gu et al., 2017). ResNet introduces residual units, which use skipped connections that model the identity function, speeding up training considerably (Gerón, 2017).

Research by Viet, Wilber, and Belongie (2016) show that such residual units avoid the vanishing gradient problem by allowing the gradient to more effectively propagate throughout the extent of the network. The network is then able to gradually restore the skipped connections as it learns the feature space. ResNet gained popularity when a 152-layer CNN trained using skip connections achieved 3.57% error on ImageNet data (He et al., 2016) and is increasingly being applied to a wide variety of tasks, including audio classification (Hershey, 2017).

### *EfficientNets & EfficientNets-Lite*

Embedded systems, such as microcomputers in robots and mobile devices do not always have the processing power to effectively use large, high-accuracy CNN architectures, such as ResNet. These low-power devices require specially optimized architectures to provide both accurate and fast inference.

Building on the efficiency gains of architectures such as MobileNetV2, Tan & Le (2019) use compound scaling to build a new family of eight scalable CNNs known as EfficientNet. Trained on the ILSVRC-2012 dataset, the baseline network, EfficientNet-B0, was developed using a multi-objective neural architecture search to optimize for accuracy and efficiency. Tan & Le's resulting architecture uses *mobile inverted bottleneck convolution* (MBConv) layers, which result in an architecture similar to that of MobileNetV2 but with compound scaling. They find that, compared to MobileNetV2, EfficientNet-B0 yields a 5.3% increase in top-1 accuracy. The largest version, EfficientNet-B7, has a top-1 accuracy of 84.4%, matching the state-of-the-art GPipe network but with 8.4-times fewer parameters and a 6.1-fold increase in speed.

In May of 2020, TensorFlow (Liu, 2020) released a family of five edge-device-optimized EfficientNets, named EfficientNet-Lite. EfficientNet-Lite modifies the EfficientNet network to allow for integer quantization and TPU compatibility, with minimal accuracy loss. Integer (*Int-8*) quantization significantly reduces the size and latency of the model, while eliminating floating-point incompatibility on many edge devices, and sacrifices only 1% of top-1 accuracy on ImageNet compared to *float-32* models (Liu, 2020). Comparing top-1 accuracy between EfficientNet-Lite and the original EfficientNet families of models, EfficientNet-Lite4, the largest of the EfficientNet-Lite models, has a top-1 accuracy of 80.2%, which is only 0.1% less than EfficientNet-B2 (Liu, 2020; Tan & Lee, 2019).

Stage $i$	Operator $\hat{\mathcal{F}}_i$	Resolution $\hat{H}_i \times \hat{W}_i$	#Channels $\hat{C}_i$	#Layers $\hat{L}_i$
1	Conv3x3	$224 \times 224$	32	1
2	MBConv1, k3x3	$112 \times 112$	16	1
3	MBConv6, k3x3	$112 \times 112$	24	2
4	MBConv6, k5x5	$56 \times 56$	40	2
5	MBConv6, k3x3	$28 \times 28$	80	3
6	MBConv6, k5x5	$14 \times 14$	112	3
7	MBConv6, k5x5	$14 \times 14$	192	4
8	MBConv6, k3x3	$7 \times 7$	320	1
9	Conv1x1 & Pooling & FC	$7 \times 7$	1280	1

**Figure 7: EfficientNet-B0 Architecture.** Resolution, number of channels, and number of layers are compound scaled for larger versions of EfficientNet. Number of layers indicates the number of sequential layers of a given operator in a stage (Tan & Le, 2019).

#### Probabilistic Approaches: Hidden Markov Models (HMM)

Hidden Markov Models (HMMs) are doubly stochastic processes based on an underlying state sequence assumed to be Markovian (Fox, 2009). HMMs have been used in many if not all speech recognition systems since the 1970s. Beginning as discrete-word, speaker-dependent systems, HMMs have gradually evolved to cover continuous-word, speaker-independent systems that can recognize large vocabularies (Gales & Young, 2008).

From Fox (2009), we begin by defining the hidden states: Let  $z_t$  denote the state of a Markov chain at time  $t$  and let  $\pi_j$  denote the state-specific transition distribution for state  $j$ . Then, for all  $t > 1$ :

$$z_t | z_{t-1} \sim \pi_{z_{t-1}}$$

We then define the initial transition distribution to determine the probability that a given state is the initial state of a sequence:

$$z_1 \sim \pi^0$$

Finally, we define the distribution of the observation  $y_t$  conditioned on the state  $z_t$  as:

$$y_t | z_t \sim F(\theta_{z_t})$$

where  $F(\bullet)$  is an indexed family of distributions for each hidden state and  $\theta_i$  are the emission parameters for state  $i$ . The resulting joint density for  $n$  observations is then given by:

$$p(z_{1:n}, y_{1:n}) = \pi^0(z_1) p(y_1 | z_1) \prod_{t=2}^n p(z_t | z_{t-1}) p(y_t | z_t)$$

To fit an HMM, we use the expectation-maximization algorithm or some sampling scheme such as Markov Chain Monte Carlo. In the former case, our objective, in simplistic terms, is to maximum the joint probability of the hidden state sequence and the data given the parameters.

In the end, we note that the advantages of an HMM for audio classification over a deep learning approach include their ability to train on and perform inference on sequences of varying length, their interpretability, and their relative efficiency on inference.

## **Methodology**

The diversity of image recognition and audio classification applications in the machine learning literature coupled with the complexity of real-time robotics tasks leads us to propose three separate approaches to a pre-specified robotics task. We begin by describing our robotics task.

### **Scavenger Hunt Challenge**

The robot is tasked with performing the Scavenger Hunt Challenge. Three separate trials of the same challenge will be performed. Each trial is set within a flat 10-square-foot space indoors, henceforth referred to as the robot's *environment*. Four cones of different colors are arranged within the *environment*, and a different object is hidden behind the green, purple, and yellow cones. The orange cone is designated as *home base*. A speaker is set up near the *environment* to broadcast sounds that the robot will identify during the challenge.

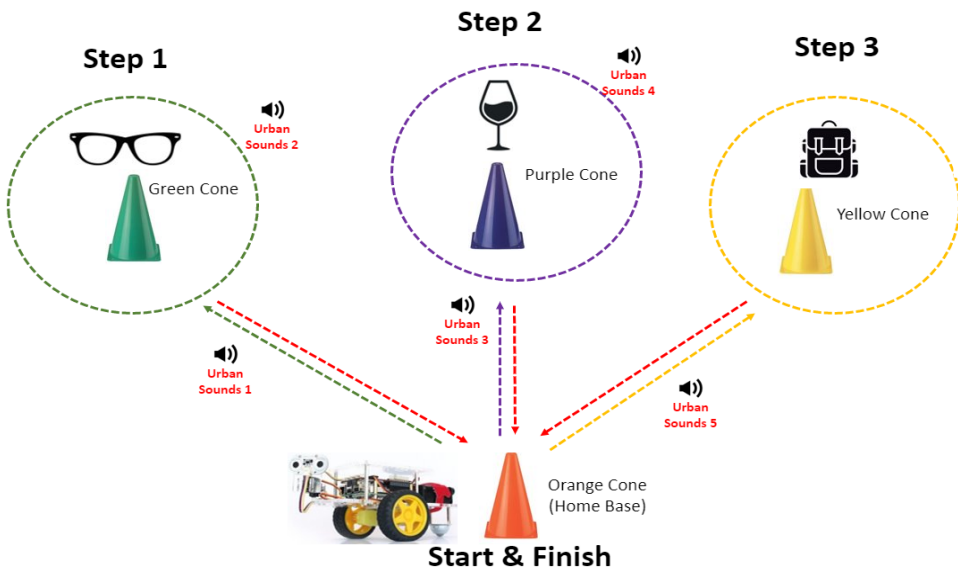


**Figure 8: Scavenger Hunt Challenge Robotics Environment**

Initially positioned within a one-foot radius of the *home base* cone, the robot is tasked with navigating to and identifying household objects placed behind the green, purple, and yellow

cones. One small, one medium, and one large object will be randomly selected from the lists in Table 1 (below) and placed behind each of these three cones prior to the start of the challenge. The robot will need to first identify the object behind the green cone, then identify the object behind the purple cone, and finally identify the object behind the yellow cone. When the object behind each respective cone is identified, the class of the object, the color of the cone it was found behind, and the time of identification must be logged. After each successive trip to the green, purple, and yellow cones, the robot must return to and orbit the *home base* cone before setting out toward the next cone in the sequence. Each of the three trials will begin by broadcasting a pitch at a predetermined frequency and will end when the robot returns to the *home base* cone for the final time.

<b>Small Objects</b>			
Tennis Ball	Dice	Eyeglasses	Banana
<b>Medium Objects</b>			
Wine Bottle	Wine Glass	Boot	Book
<b>Large Objects</b>			
Suitcase	Backpack	Tennis Racket	Bicycle Helmet

**Table 1:** List of 12 possible classes of objects to be hidden behind the cones during the challenge. The objects are further divided into three parent classes: small, medium, and large objects.

Concurrently, five sounds from the *UrbanSound8K* dataset<sup>3</sup> (Salamon, Jacoby, & Bello, 2014) will be played from a nearby speaker at 8 kHz at random times throughout the trial. When

---

<sup>3</sup> More information about the *UrbanSound8K* dataset can be found in the *Data* subsection.

each sound is played, the robot will be required to identify the sound class and log the time the classification was made. The five sounds will be selected at random from four of the following 10 sound classes:

<b><i>UrbanSound8K Classes</i></b>	
Gun Shot	Drill
Dog Bark	Jackhammer
Car Horn	Children Playing
Street Music	Engine Idling
Air Conditioner	Siren

**Table 2: *UrbanSound8K Classes***

## *Robotics Hardware and Software*

Each trial has the following hardware specifications:

	Trial I	Trial II	Trial III
<b>CPU:</b>	Raspberry Pi 4 Model B, 4GB of RAM		
<b>Robotics Platform:</b>	Dexter GoPiGo3 Base Kit		
<b>Hard Disk:</b>	MicroSD Card, 32 or 64 GB		
<b>Distance Sensor:</b>	1 x Dexter Distance Sensor		
<b>Camera:</b>	1 x Raspberry Pi Camera		
<b>Batteries:</b>	8 x AA Batteries		
<b>Servo:</b>	1 x Dexter Servo Kit		
<b>Microphone</b>	1 x SiZheng Omnidirectional USB Microphone	1 x TKGOU Gooseneck Omnidirectional Condenser USB Microphone	1 x TKGOU Gooseneck Omnidirectional Condenser USB Microphone
<b>Accelerator (Optional):</b>	Intel Neural Compute Stick	Google Coral USB Edge TPU	None

**Table 3: Trial Hardware Specifications**

Each trial has the following software specifications:

	Trial I	Trial II	Trial II
<b>Operating System:</b>	Raspbian Buster, 64-Bit		
<b>Python:</b>	Version 3		
<b>Deep Learning Framework:</b>	TensorFlow 2+	TensorFlow 2+ (training); TensorFlow Lite (inference)	PyTorch (audio classification); TensorFlow 1.15 (object detection)

**Table 4: Trial Software Specification**

#### *Training Data*

We use transfer learning to obtain pre-trained models for the trials in which we rely on CNNs for object detection and/or audio detection tasks. The YOLOv3 and MobileNetV2 SSD object detection models were pre-trained on the Common Objects in Context (COCO) dataset (Lin et. al, 2015). This is an object detection, segmentation, and captioning dataset of 1.5 million training instances with five captions per image and bounding boxes around the objects in each image, allowing users to train on objects in a variety of contexts. ResNet and EfficientNet-Lite image recognition models were pre-trained on ILSVRC-2012.

For the object detection tasks, we then further train our models to recognize the 12 object classes and four colored cones of the Scavenger Hunt Challenge. For the 12 object classes, additional bounded images were obtained from the Google Open Images Dataset. Images of the colored cones were manually captured, and bounding boxes were subsequently added.

For the audio detection tasks, we use data from the *UrbanSound8K* dataset (Salamon, Jacoby, & Bello, 2014). This dataset consists of 8,732 sound recording excerpts taken from 1,302 original recordings organized into 10 classes (see Table 2). The recording excerpts range

in length from one to four seconds, and most recordings were recorded in stereo at 44.1 kHz. In addition, the recordings are divided into 10 stratified folds for cross-fold validation. The predefined folds ensure that all of the excerpts from a given original sound file are contained in the same fold, thus avoiding any data leakage between training and validation.

Figure 9 contains a sample of *mel spectrogram* images for each of the 10 classes of the *UrbanSound8K* dataset. We see significant diversity of spectrograms within each class and noticeable similarity of spectrograms across the classes in certain cases, underscoring the difficulty of this classification task.

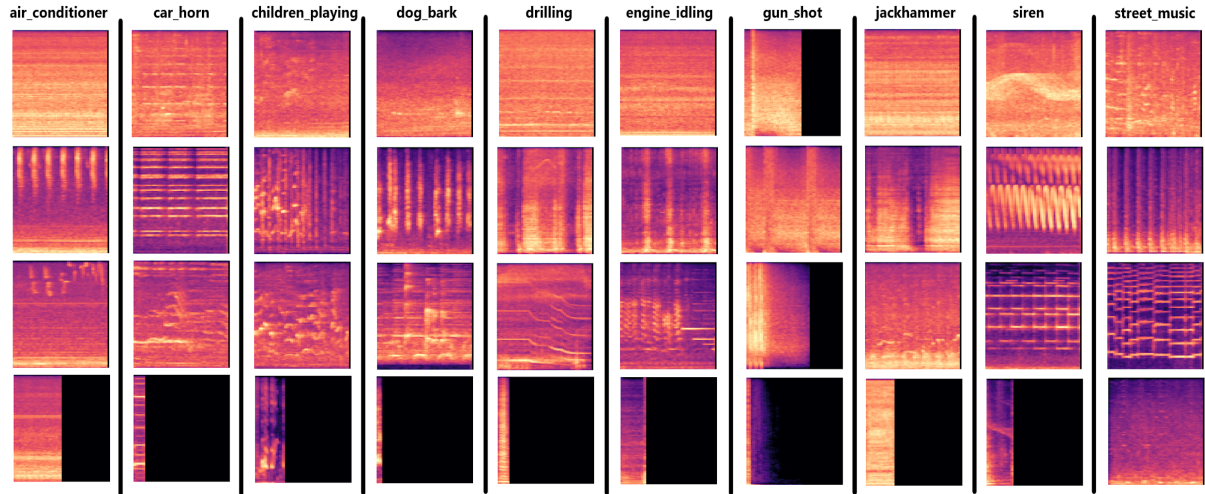


**Figure 9: Mel spectrogram images of UrbanSound8K classes**

During the robotics challenge, the audio signals obtained by the robot's microphone in its *environment* are constantly being augmented by the sounds of the robot – the activation of the motors and wheels, the buzzing of the servos, and the humming of the CPU. Given this constant noise, additional data augmentation and/or filtering measures are proposed in each trial below.

## Trial I Models

### *Object Detection*

Trial I uses OpenCV package (Bradski & Kaehler, 2008) for cone detection. We first convert an RGB input image to a Hue Saturation Value (HSV) image. Unlike RGB, which is defined in relation to primary colors, HSV is defined in a way that is similar to how humans perceive color. Under the HSV framework, *hue* encodes color information, where zero degrees corresponds to the red, 120 degrees corresponds to the green, and 240 degrees corresponds to the blue color on the color wheel. *Saturation* encodes the intensity or purity of a color, where for example, pink is less saturated than pure red. *Value* encodes the brightness of color, including shading and gloss components.

To filter for a particular color, we specify a range on the color wheel for said color. After we apply this filter, we then remove noise via *erosion* and *dilation*. The former decreases the size of objects and removes small anomalies by subtracting objects with a radius smaller than the structuring element. The latter increases the size of objects, filling in holes and connecting disjointed areas that are smaller than the size of the structuring element.

Next, we apply a *median blur* to smoothen the image, which helps display the object of interest more clearly, and then a *Canny edge detection* technique to find the edges of the object of interest. At this point, the object will look more like a cone-shaped triangle.

Finally, we identify the contours of the image. Contours can be explained simply as a curve joining all the continuous points along a boundary, having the same color or intensity. We apply an approximate polygon technique to the objects of interest. This provides a more angled structure to the object. We apply *convex Hull* to specifically isolate cone-shaped objects.

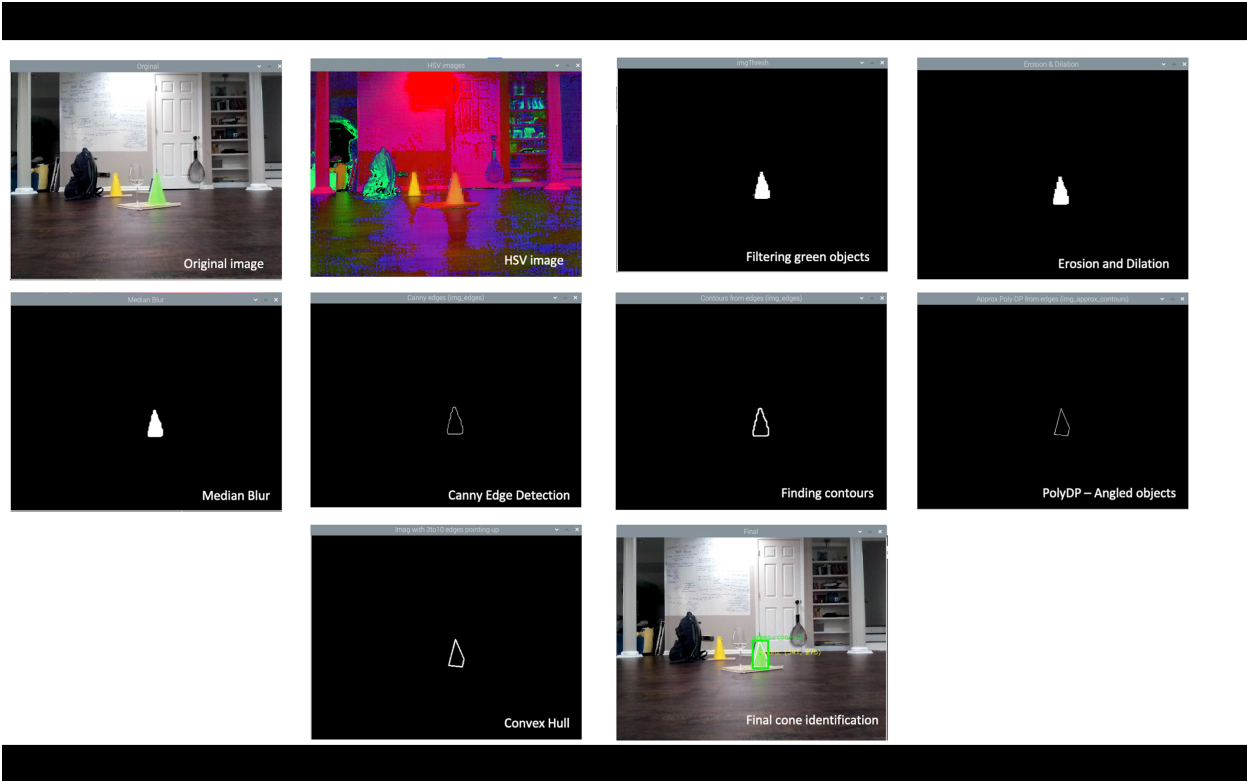


**Figure 10: Cone detection with OpenCV**

Trial I employs a pre-trained MobileNetV1 SSD for object detection. As previously discussed, MobileNet SSD is well-suited for real-time object detection given its speed and accuracy on relatively low-powered devices such as the Raspberry Pi 4. Also, unlike YOLOv3, it is easy to implement on the Raspberry Pi 4 with an *Intel Neural Compute Stick* (NCS) accelerator. To implement MobileNet SSD on the Raspberry Pi 4, we first need to create an environment compatible with our NCS. Intel developed the *OpenVINO* toolkit that allows for accelerated computing in its NCS devices. This toolkit and its dependencies are downloaded and configured to create the process of passing object detection tasks through the USB port into the NCS. We subsequently activate the *OpenVINO* environment, download the pre-trained MobileNet SSD model weights, class labels, and model configuration, and compile the weights and configuration files (Rosebrock, 2018).

On implementation, MobileNet SSD automatically filters out inferences below a certain confidence threshold, constructs labeled bounding boxes around the objects detected in the image, and displays the resulting frame with class labels, bounding boxes, and prediction probabilities.

### *Audio Classification*

Trial I uses an HMM for the audio classification component of the Scavenger Hunt Challenge. As previously mentioned, one of the principal advantages of using HMMs for audio classification is that they can be trained on and tested with audio sequences of varying lengths. On the other hand, one of the disadvantages of HMMs in general is that they require the user to decide *a priori* the number of hidden states that compose the model. To attempt to remedy this, we employ *Self-Organizing Maps* (SOM) (Kohonen, 2001).

SOMs are a special class of neural networks used for unsupervised learning. SOMs are particularly adept at transforming high-dimensional, non-linear data into a low- (typically two) dimensional representation, preserving the topology of the original feature space (Asan & Ercan, 2011). As such, they present a useful unsupervised approach to determining *a priori* the number of hidden states.

We train one SOM for each of the 10 audio class labels. Moreover, in order to make our models robust to noise, we make two copies of the original 8,732 training instances and randomly mix them with pre-recorded robot noise resulting in approximately 26,000 training samples, 8,732 of which remained unchanged. We also maintain one corpus of training data where each recording is held at a 44.1 kHz sampling rate, and we create an additional copy of the entire training corpus where each sample recording is down-sampled to 22 kHz. Last, we convert all sample audio signals to MFCCs with 13 cepstral coefficients.

Training SOMs is a balance between reducing both topographic error and quantization error (Asan & Ercan, 2011), among other measurements. Given a map of  $N$  nodes, quantization error measures the average Euclidean distance between a training instance and its Best Matching Unit (BMU) node.<sup>4</sup> Topographic error, on the other hand, measures one minus the percentage of BMUs and second-BMUs that are adjacent in the node map. As such, such a measurement is appropriate for approximating topographical preservation of the original high-dimensional representation of the data. Furthermore, while quantization error decreases monotonically with the number of training iterations, topographical error behaves more erratically. In the end, we find that training on 20 iterations consistently produced sufficiently low topographical error (less than 0.17 for nearly every label) and quantization error.

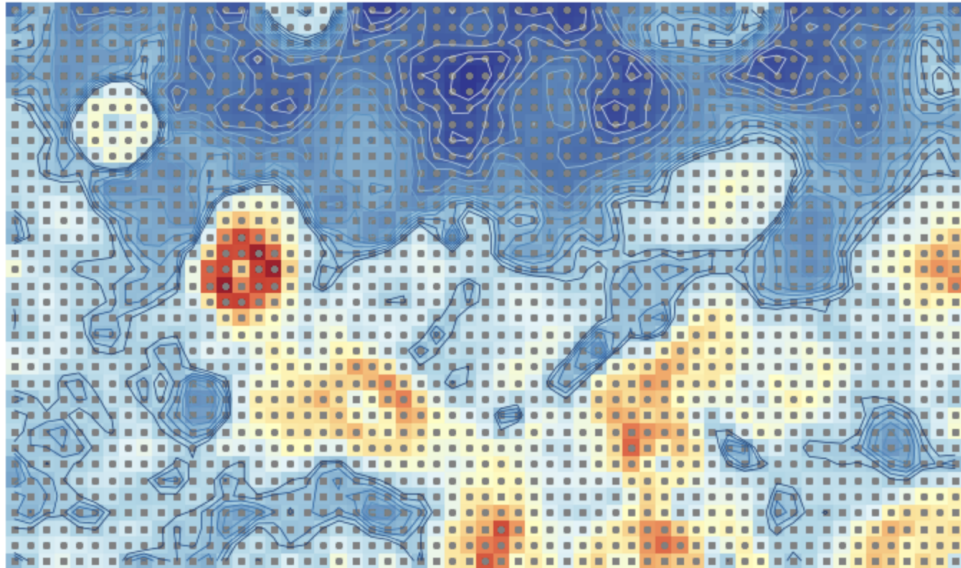


**Figure 11: Contour plot of SOM for the “street music label”.** Dark colors represent ‘hills’ where adjacent nodes are far apart in Euclidean terms and bright colors represent ‘valleys’ where adjacent nodes are very close together.

---

<sup>4</sup> For more details on the SOM training algorithm, see Asan & Ercan, 2011.

In the absence of a clear objective function, unsupervised approaches such as SOMs do not produce unequivocal conclusions as to the ideal number of hidden states given a training set of MFCCs. That said, they can help indicate the complexity of the state space of one MFCC training set relative to the others. As such, we use observations from each SOM contour plot to better inform our decision as to the appropriate number of hidden states when training our HMMs for each audio label.

Given the ambiguity as to the appropriate number of hidden states, the effect of the sampling rate, and other hyperparameters such as the distributions of the hidden states, we opt to train a number of HMMs for each audio label and compare their recall scores:

<b>Hyperparameters</b>	<i>Number of Hidden States</i> (1)	12	Various	Various	Various
	<i>Sampling Rate</i>	40kHz	40kHz	40kHz	20kHz
	<i>Hidden State Distribution</i> (2)	Gaussian: Univariate	Gaussian: Multivariate	Gaussian: Multivariate	Gaussian: Multivariate
	<i>EM Iterations</i> (3)	200	2	50	250
<b>HMMs</b>	<i>Car Horn</i>	0.517510	<b>0.521401</b>	0.489637	0.501946
	<i>Children Playing</i>	<b>0.721667</b>	0.293333	0.413333	0.440833
	<i>Engine Idling</i>	0.501667	0.708333	<b>0.757778</b>	0.728333
	<i>Drilling</i>	0.511667	0.745000	<b>0.777778</b>	0.700000
	<i>Siren</i>	0.533214	0.601436	<b>0.771531</b>	0.659785
	<i>Gun Shot</i>	<b>0.691964</b>	0.256696	0.255952	0.272321
	<i>Street Music</i>	0.446667	0.656667	<b>0.754444</b>	0.689167
	<i>Air Conditioner</i>	0.343333	<b>0.790833</b>	0.671111	0.694167
	<i>Jackhammer</i>	0.728333	0.843333	<b>0.850000</b>	0.832500
	<i>Dog Bark</i>	0.485000	0.806667	0.747778	<b>0.813333</b>

**Table 5: HMM recall scores for each audio label-specific HMM.** (1) When the table above indicates “various” hidden states, each label-specific HMM employed a different number of hidden states based on the SOM contour plots. (2) Univariate Gaussian distributions for the hidden states were used in cases when a single MFCC window was fed into the model as a training instance; multivariate Gaussian distributions were used in cases where MFCC windows for an entire sample audio recording were concatenated row-wise and fed into the model as a training instance. Thus, in the latter case, a single time step was multidimensional. (3) Each

HMM was trained using the expectation-maximization (EM) algorithm and validated by finding the highest log likelihood amongst all 10 HMMs given the validation sample.

As can be seen in Table 5, each audio label-specific HMM performs differently depending on the hyperparameters chosen. Thus, on implementation, we choose the 10 best-performing audio label-specific HMMs highlighted above.

Finally, we propose a simple criterion with which the robot will perform an audio classification inference using the data collected from the microphone's audio stream. Using a two-minute sample of robot noise, we measure the mean decibel level. We then choose an arbitrary threshold above this mean based on our observations of the decibel levels of concurrent robot noise and urban sounds broadcast from our speaker. On implementation, only when the decibel level surpasses this threshold does the robot send an audio sample from the stream to the HMM for inference.

## Trial I Robotics Implementation

Real-time implementation of Trial I models is performed via five separate threads on the Raspberry Pi 4:

- *Thread 1: Main*
  - Controls robot locomotion and other movements.
  - Starts all other threads as needed.
- *Thread 2: Camera Feed*
  - Initializes and warms up the camera.
  - *Thread 1: Main* pushes images from *Thread 2: Camera Feed* to *Thread 3: Object Detection* queue.
  - *Thread 5: Live Video Feed* uses frames from *Thread 2: Camera Feed* to show a live feed to the user while the robot is moving.
- *Thread 3: Object Detection*
  - Pushes the object detection model on to the TPU.
  - *Thread 1: Main* captures pictures using *Thread 2: Camera Feed* and pushes the saved images path to the *Thread 3: Object Detection* queue.
  - Monitors its queue for any input image on which to perform inference. When an input image enters the queue, pushes the image to the TPU for inference and logs

the results.

- *Thread 4: Audio Detection*
  - Collects data streamed from microphone. If streamed audio data surpasses a predetermined decibel threshold, performs inference using the audio detection model and logs the results.
- *Thread 5: Live Video Feed*
  - Displays live feed using frames called from *Thread 2: Camera Feed*.

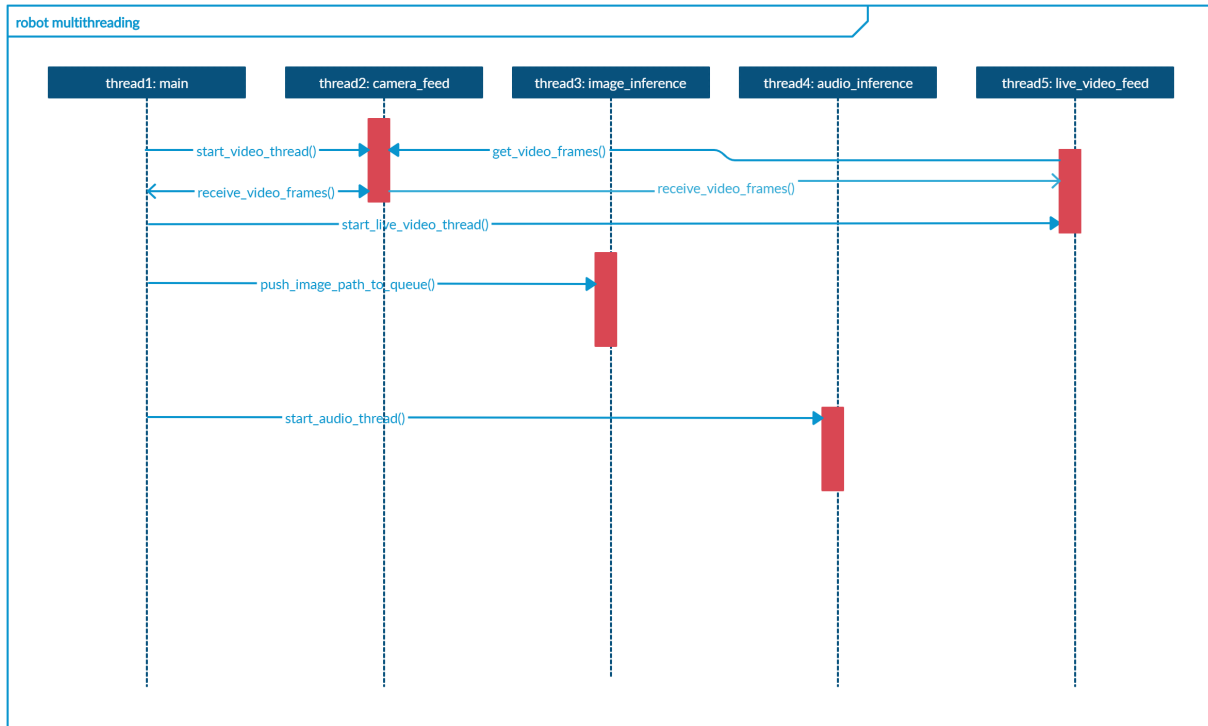


**Figure 12: Trial I multithreading schema**

## Trial II Models

Trial II seeks to find the most efficient deep learning approaches to real-time object detection and audio classification. As such, we select models that can be converted to the lightweight TensorFlow Lite framework, making them both integer-quantizable and TPU-compatible. This significantly reduces model size, inference time, and framework dependencies.

### *Object Detection*

Trial II uses MobileNetV2 SSD for both object and cone detection. Unlike YOLOv3, MobileNetV2 SSD is compatible with the Google Coral USB Edge TPU, which we find can increase inference speeds by a factor of 10. Using MobileNetV2 SSD, we can thus minimize object detection inference times and free up compute resources for the other components of the Scavenger Hunt Challenge. We note that although the TPU does increase power requirements, there was no obvious negative impact on overall operations during the Scavenger Hunt Challenge.

We retrain the last four layers of two separate MobileNetV2 SSD models, respectively: one model to detect the cones and the other to detect the objects behind each cone. This ensures that both models are optimized for their respective objectives. To train our cone detection model, we captured 200 images of different colored cones using the Raspberry Pi camera and manually labelled them with bounding boxes. To train our object detection model, we used 1,500 additional images of the 12 Scavenger Hunt Challenge objects and their corresponding bounding boxes from the Google Open Images Dataset.

Out-of-sample recall scores for the object detection model are below. Not included are the results of the cone detection model, though we note that out-of-sample recall scores for cone detection surpassed 90%.

Type	Object Class	Validation Recall
Large	Suitcase	85.0%
	Backpack	81.2%
	Bicycle Helmet	87.4%
	Tennis Racket	95.0%
Medium	Book	79.5%
	Boot	95.5%
	Bottle	85.0%
	Wine Glass	93.9%
Small	Dice	99.2%
	Glasses	70.3%
	Tennis Ball	97.2%
	Banana	92.3%

**Table 6: MobileNetV2 SSD validation recall scores**

#### *Audio Classification*

Trial II uses an EfficientNet CNN for audio classification and takes a filter-first approach to the training and signal processing. As such, the model is trained on unaltered *UrbanSound8K* data, and during the robotics challenge, the robot's operating noise is filtered in real-time.

In order to mirror the pre-processing of the sound files to be broadcast during the Scavenger Hunt Challenge, we pre-process the *UrbanSound8K* audio files by converting them to mono, down-sampling them to 8 kHz, and applying peak normalization. The signals are then

zero-right-padded to the maximum length of four seconds. Finally, each padded signal is converted into a *mel spectrogram* image of shape (300, 300, 3) with an FFT window length of 2,048 and 512 hops between successive frames. The 10 folds from the original data set are kept and used for cross-validation.

We use an EfficientNet-Lite4 CNN pre-trained on ILSVRC-2012 data to classify the *mel spectrogram* images. Since the *UrbanSound8K* dataset contains 10 new classes, we apply a new classification header to the frozen feature vectors<sup>5</sup>. The classification header consists of a 0.2 dropout layer followed by a dense layer using softmax activation with an L2 regularization factor of 0.0001. The model is then quantized and converted to a TensorFlow Lite model.

Training of the classification header netted a 10-fold cross-validation top-1 accuracy of 78%. The resulting model is also two times faster on inference than a similarly-trained ResNet-34 model, with only a two percent difference in top-1 accuracy on the *UrbanSound8K* data. Table 7 shows the out-of-sample metrics for one of the 10 validation folds.

---

<sup>5</sup> Although we experimented with unfreezing some of the top pre-trained layers, which resulted in higher top-1 accuracy scores, this had to be abandoned due to issues with quantization.

Audio Class	Precision	Recall	F1-Score
Air Conditioner	0.59	0.78	0.67
Car Horn	0.87	0.92	0.89
Children Playing	0.80	0.88	0.84
Dog Bark	0.75	0.93	0.83
Drilling	0.67	0.55	0.60
Engine Idling	0.86	0.52	0.65
Gun Shot	0.78	0.91	0.84
Jackhammer	0.84	0.80	0.82
Siren	0.85	0.91	0.88
Street Music	0.84	0.69	0.76
<b>Top-1 Accuracy</b>	<b>0.77</b>		

**Table 7: EfficientNet-Lite4 fold-1 validation metrics**

#### *Real-Time Audio Signal Processing and Noise Filtering*

We begin the audio filtering process by analyzing the volume of the real-time audio stream, with the aim of recording data from the audio stream only when a certain volume threshold is surpassed. The audio stream is sampled at 44.1 kHz. We analyze the byte stream in chunks of 4,096 values, equivalent to roughly a tenth of a second. An effective way to measure the volume or energy of a particular audio stream chunk is to calculate its root mean square (RMS). The RMS calculation is effective since it requires the squaring of all integer values, which will give equal weight to the positive and negative signal values. The mean RMS value of our sample recording of typical robot noise is less than 2,000 with a standard deviation of 250. As a result, we set the threshold for triggering a recording to be a chunk with an RMS value that exceeds 3,000. Figure 13 depicts a four-second recording of a sample ‘dog bark’. We see four

instances – each a separate bark – where the RMS of the chunk exceeds the typical robot noise threshold (red dashed line). When this happens, a 4.5-second recording begins from when the threshold is first exceeded. Since the urban sound samples are no more than four-second-long, we use the last 0.5 seconds of the recording as the noise sample for filtering. This is useful because the exact character of robot noise depends on what the robot is doing when the urban sound sample is broadcast.

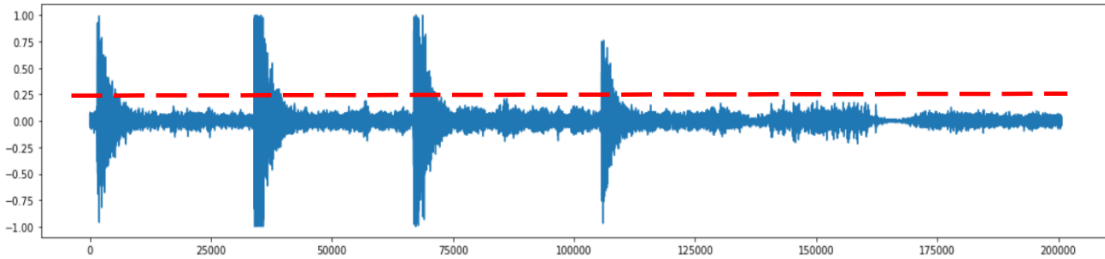


**Figure 13: Dog bark decibel levels versus RMS-determined noise threshold**

We next propose a filtering technique for removing the ambient robot noise. We choose a spectral gating noise reduction algorithm originally proposed by the Audacity Team (2015). Spectral gating selectively filters the unwanted ambient noise while attempting to maintain the integrity of the target sound signal. Spectral gating takes two audio files as inputs: the raw audio segment to be filtered and a sample of the noise that we want removed from the raw segment. The result of the algorithm is a cleaned signal.

The algorithm begins by performing a Fourier transform of the noise signal, binning it into 1,025 distinct frequency bands. It then calculates the mean and standard deviation power for each frequency band. The resulting metrics will be used to calculate a threshold that represents the peak power of noise expected at each frequency band (Figure 14). The aforementioned process is also applied to the raw signal to be filtered.

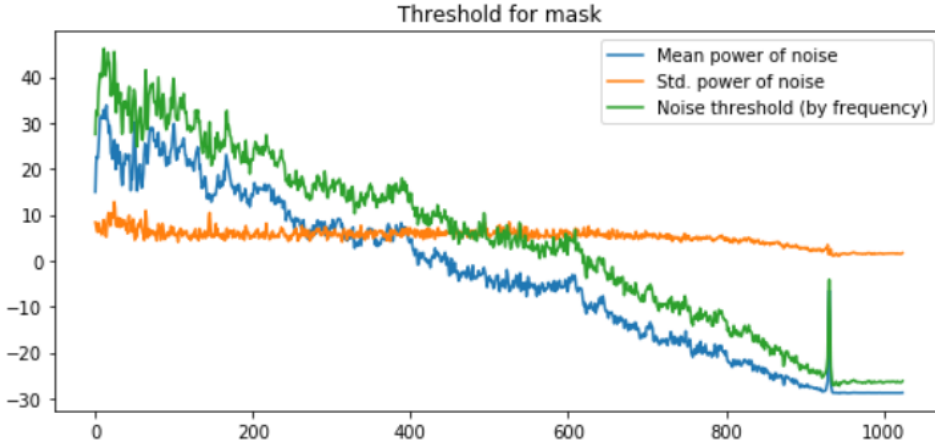


**Figure 14: Noise power metrics by frequency band.** The x-axis represents the count of frequency bands while the y-axis represents the power of the noise signal at each frequency band. The noise has higher power at lower frequencies and lower power at higher frequencies. The standard deviation of the noise is relatively small and consistent. We can also see a low power but distinct signal coming from the motors at a high frequency bin.

Next, the algorithm develops a filtering mask. The mask is built by comparing the original mean signal power at each frequency band to the noise threshold at each frequency band. If the power of the noise threshold is greater than the mean power of the original signal, then the frequency bin becomes part of the mask. This process is conducted separately for all frequencies at all time windows of the original signal. The previous step ensures that the mask is dynamic over time, meaning that certain frequencies are omitted from the mask at certain time periods when there are strong signals that are not suspected to be noise. The filtering algorithm smooths the mask over frequency and time, ensuring there are no sharp cutoffs or losses and that some portions of noise and signal will be able to bleed into the recovered signal.

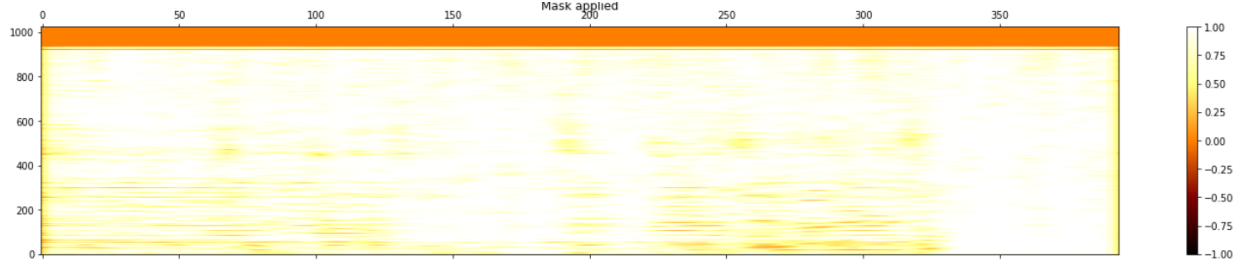


**Figure 15: Temporal spectral density of mask.** The first portion of the signal has some unmasked portions seen, followed by a short pause where nearly everything is masked and then more signal is unmasked. The final portion of the clip seems to have no signal and is completely masked. There is also a clear mask at the high frequency bin where we anticipate a faint motor noise.

Finally, the algorithm applies the mask to the original signal over the time windows in the frequency domain. The resulting spectrogram is depicted at the bottom of Figure 16. Figure 16 compares the spectrogram of the filtered signal to the spectrograms of the original recording and the signal from the *UrbanSound8K* dataset. We see in the unfiltered spectrogram that much of the definition of the urban sound sample is obfuscated by the robot noise during the recording process. Filtering allows us to recover the definition and overall sonic characteristics of the urban sound sample, which can be confirmed by listening to the filtered sound. Much of the high-frequency definition (the top of the spectrogram) is lost, due to the compound effect of three factors: 1) the robot motor noise containing similar high frequencies, 2) the limited recording quality of the microphone and broadcast quality of the speaker, and 3) the decay of high-frequency sounds across distances when broadcast from the speaker.

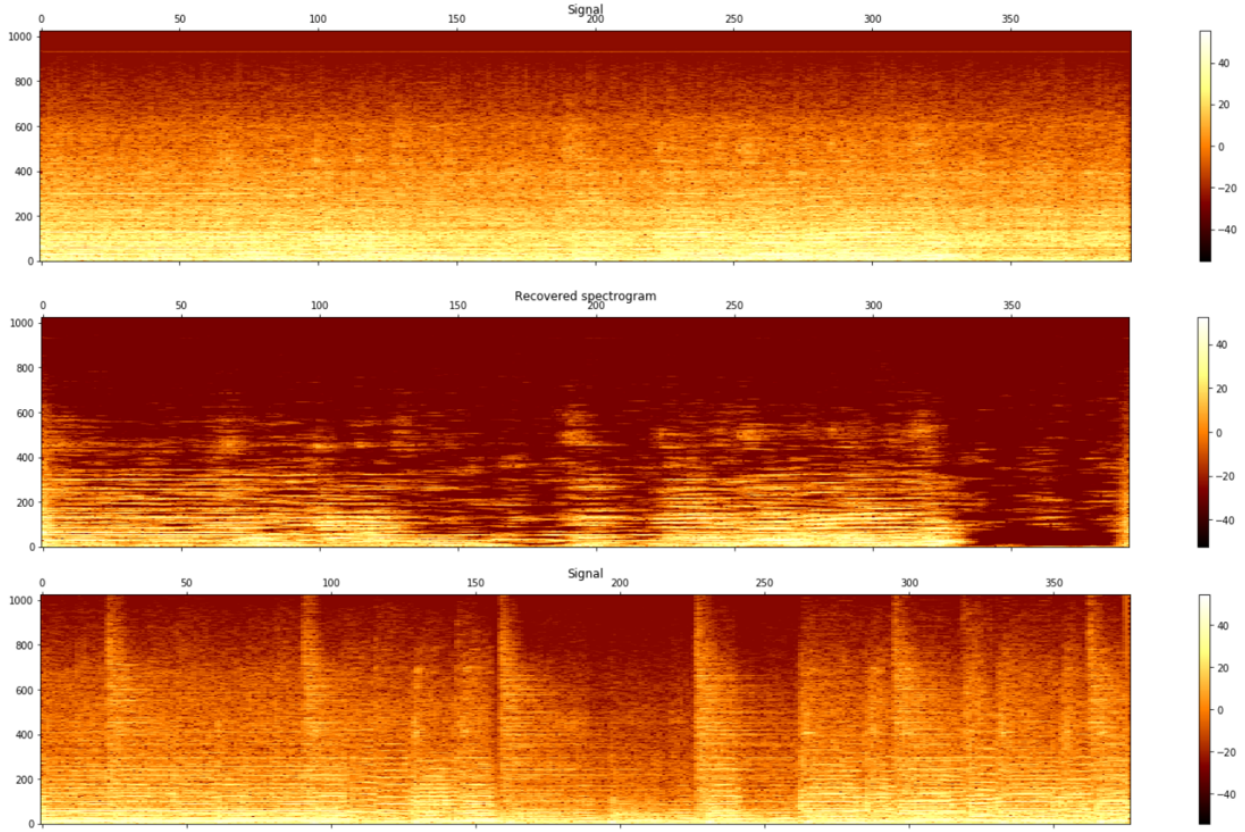


**Figure 16: Temporal spectral densities in comparison.** Temporal spectral densities of the raw recording (top), recovered signal after noise filtering (middle), and the original four-second audio clip from the *UrbanSounds8k* dataset (bottom).

Since the audio model requires a different spectrogram resolution than the noise filtering algorithm, we ultimately inverse Fourier transform the filtered spectrogram back to the time domain and pass on this result to the audio model for *mel spectrogram* conversion and inference.

### Trial II Robotics Implementation

Trial II uses a multithreading approach for implementation. This allows the robot to drive, identify objects, and recognize sounds. We chose multithreading over multiprocessing after preliminary tests indicated that multiprocessing was not well supported on our hardware and software configurations. Real-time implementation of Trial II models was performed using three separate threads on the Raspberry Pi 4:

- *Thread 1: Main - Controls and Locomotion*

- Operational control for the scavenger hunt and initialization of other threads.
  - Directs robot speeds and movements based on programmed hunt objectives and responses from the cone detection model in *Thread 2*.
- *Thread 2: Cone and Object Detection*
  - Controls the capture and processing of images and video from the camera.
  - Sends images to the cone detection model on the TPU for inference and returns the relative position of the desired cone (if found) to *Thread 1*.
  - Sends video frames to the object detection model on the TPU for inference and returns the class of the hidden object (if found).
  - Logs timing and results of cone and object detection.
- *Thread 3: Audio Detection*
  - Initiates and controls continuous collection and processing of audio.
  - Sends filtered recordings to the audio detection model on CPU for inference and returns the predicted class of the recorded sound.
  - Logs timing and classification of audio events.

### Trial III Models

#### *Object Detection*

For cone detection, Trial III employs YOLOv3 via the Keras API for transfer learning, freezing the first 249 of 252 total layers and fine-tuning the model on a set of 500 manually captured and labeled images of orange, green, yellow, and purple cones in surroundings similar to those of the robotics *environment*. Altogether, the YOLOv3 fine-tuning process consists of 100 epochs with early stopping and takes approximately 22 hours.

The bounding boxes from YOLOv3 inferences can be used to help the robot locate and navigate to the cones. We can derive the angle and distance from the robot to the cone using the bounding box coordinates and the properties of triangle similarity. Indeed, we find that calculating the angle of attack and distance in such a way is preferred over the GoPiGo3 distance sensor given the relative inaccuracy of the sensor.

During the Scavenger Hunt Challenge, the robot needs to know the approximate distance from and angle to the cone. Let  $F$  be the focal length of the camera,  $P$  be the width of the pixels

of the cone calculated from bounding box coordinates,  $D$  be the distance to the cone, and  $W$  be the actual width of the cone (5.5 inches for the Scavenger Hunt Challenge). Triangle similarity is then calculated as:

$$F = \frac{P * D}{W}$$

Next, we propose the below equation to measure the angle of attack from the robot to the cone. Let  $I$  be the center of the image and  $C$  be the center of the predicted cone, measured in pixels. We divide the difference between  $I$  and  $C$  by a constant<sup>6</sup>. A positive result indicates a clockwise rotation and a negative result indicates a counterclockwise turn:

$$R = \frac{|I - C|}{12}$$

We opted not to perform cone detection inferencing using the Google Coral USB Edge TPU. This is because we found the Keras API to be a necessary component of this implementation, given the ease with which it can translate the original Darknet implementation of YOLOv3 into Python. That said, unfortunately, Keras made converting the model to the TFLite format required by the Coral Edge TPU infeasible because of the potential information loss when the original weights are quantized.

We use an ensemble approach for inference, where the robot captures 10 images per inference and selects the class predicted for the majority of the 10 images. The model has an average inference time of 1.55 seconds and a mAP of 87%.

For object detection, we use MobileNetV2 for transfer learning. The benefits of the MobileNetV2 model include high accuracy and inference speed on the Coral Edge TPU. Training the model took approximately 10 hours for 100 epochs with early stopping after

---

<sup>6</sup> We determined that a horizontal movement of 12 pixels was equivalent to a GoPiGo3 rotation of one degree.

freezing the first 50 of 53 total layers. For our training data, we downloaded 500 open source images representing our 12 Scavenger Hunt Challenge objects and manually labeled them.

Because MobileNetV2 can be converted to a TensorFlow Lite format, we use the Coral Edge TPU to speed up our inferences. As with the cone detection model, an ensemble approach is used for inference. The robot takes 10 images and then selects the class predicted for the majority of the 10 images. The model achieves an average inference time of 330 milliseconds and a mAP of 91%.

#### *Audio Classification*

For audio classification, Trial III uses transfer learning from a ResNet-34 CNN pre-trained on ImageNet data, which we find to be more effective than training a CNN on audio data from scratch. We implement ResNet-34 using the FastAI package built on PyTorch. We first train the head to make predictions on the 10 audio classes from the *UrbanSound8K* dataset, and then we unfreeze the remaining layers of the model and train the entire model. We use FastAI's *fit\_one\_cycle* option, which uses a cyclical learning rate in which the learning rate starts at some arbitrarily low value, increases to a predetermined max value, and then decreases to zero. Training at a cyclical learning rate has been shown to require fewer epochs to adequately train (Smith, 2017).

Prior to training, we augment *UrbanSound8K* data with noise generated from the GoPiGo3 while navigating the robotics *environment*. The volume of the robot noise is adjusted such that the urban sound samples are still audible after mixing by adjusting the robot noise to have the same max volume as each urban sound sample. After mixing the sounds, we convert them to mono and down-sample to an 8 kHz sampling rate. The clean urban sound samples as

well as the augmented urban sounds are converted into *mel spectrogram* images and used to train the ResNet-34 CNN. Table 8 shows the fold-1 validation metrics.

Audio Class	Precision	Recall	F1-Score
Air Conditioner	0.75	0.71	0.73
Car Horn	0.95	0.89	0.92
Children Playing	0.86	0.73	0.79
Dog Bark	0.80	0.87	0.83
Drilling	0.74	0.77	0.76
Engine Idling	0.91	0.71	0.80
Gun Shot	0.94	1.00	0.97
Jackhammer	0.78	0.94	0.85
Siren	0.89	0.94	0.91
Street Music	0.85	0.89	0.87
Accuracy			0.83

**Table 8: ResNet-34 fold-1 validation metrics**

Similar to Trial I, on implementation, sound is captured for inference from the real-time audio stream only when a certain volume threshold is exceeded.

### Trial III Robotics Implementation

Real-time implementation of Trial III models is performed via three separate threads on the Raspberry Pi 4:

- *Thread 1: Signal Detection, Object Detection, and Robot Movements*
  - Waits for signal to start robot.
  - When signal is detected, initiates cone detection and robot movement program.
  - Sends cone location data to movement class, which directs robot to each respective cone.

- When the robot is in position behind each target cone, detects objects and logs the results.
- *Thread 2: Audio Recording*
  - Collects data streamed from microphone. If streamed audio data surpasses a predetermined decibel threshold, saves recording of audio to file.
- *Thread 3: Audio Classification*
  - Performs inference using the audio classification model and logs the results.

## Findings

### Trial I

For Trial I, the robot was able to accurately classify the medium and large-sized objects. Nevertheless, it struggled to classify the eyeglasses. This may be because MobileNetV1 often struggles to identify smaller objects vis-a-vis approaches such as YOLOv3. It also may be because our MobileNetV1 SSD was not trained on standalone eyeglasses, but rather eyeglasses worn on a face.

Trial I Results					
Object Detection			Audio Classification		
Timestamp from Start (ms)	Prediction	Actual	Timestamp from Start (ms)	Prediction	Actual
59,449	Wine Glass	Eyeglasses	61,123	Dog Bark*	Dog Bark
143,180	Wine Glass	Wine Glass	160,258	Car Horn*	Car Horn
238,464	Backpack	Backpack	200,860	Children Playing	Street Music
281,409	End at Orange Cone		245,878	Children Playing	Gun Shot
			259,458	Car Horn	Siren

**Table 9: Trial I Results.** \*Although the HMM was consistently able to correctly classify Dog Barks and Car Horns during preliminary tests on live-streamed audio data, given the unusual timestamps recorded from Trial I, we cannot unequivocally affirm that those two audio classes were correctly inferred.

Trial I's HMM performs inference efficiently but was unable to classify certain sounds (e.g. Gun Shot and Drilling) and often struggled to differentiate other sounds (e.g. Children

Playing versus Street Music and Car Horn versus Siren). That said, the aforementioned sounds that it struggled to differentiate often had noticeably overlapping features. For example, the sounds of traffic could be heard in many of both the Siren and Car Horn samples of the *UrbanSound8K* dataset. Finally, we were unable to get consistent decibel readings with which to reliably trigger audio classification when (and only when) an urban sound sample was broadcast from our speaker. We note that while Trial I employed a flat, tabletop omnidirectional microphone, Trials II and III both employed a gooseneck omnidirectional microphone. Indeed, the extra proximity of the tabletop microphone to the robot noise may have made getting consistent decibel readings more difficult.

## **Trial II**

For Trail II, the robot successfully navigated the course with limited errors. The large, medium, and small hidden objects were correctly classified, with one caveat: the eyeglasses were only identifiable when placed on an image of a face. This is because all of the eyeglasses samples in the training data were of eyeglasses worn on a face.

Trial II Results					
Object Detection			Audio Classification		
Timestamp from Start (ms)	Prediction	Actual	Timestamp from Start (ms)	Prediction	Actual
31,577	Eyeglasses**	Eyeglasses	14,349	Dog Bark	Dog Bark
86,983	Wine Glass	Wine Glass	32,423	Car Horn	Car Horn
139,538	Backpack	Backpack	58,219	Street Music	Street Music
156,255	End at Orange Cone		77,971	Dog Bark	Gun Shot
			101,102	Siren	Siren

**Table 10: Trial II Results.** \*\*Eyeglasses were placed on an image of a face during the challenge

The Trial II audio model successfully classified four out of five urban sounds played during the change, misclassifying only the Gun Shot as a Dog Bark. This is possibly due to the short length of the single-shot Gun Shot sample. In general, the audio model was less reliable at classifying shorter sounds, which is not surprising since the spectrograms corresponding to the shorter sound samples were right-zero padded and CNNs often struggle with correctly learning information at the edge of images.

### Trial III

For Trial III, the robot successfully classified every object except for the eyeglasses. The audio model successfully classified the Dog Bark, Car Horn, and Street Music samples, but

failed to distinguish the Children Playing from the Gun Shot samples and the Drilling from the Siren samples. Thus, although the Trial III’s ResNet outperformed Trial II’s EfficientNet-Lite4 during validation in terms of top-1 accuracy, EfficientNet-Lite4 performed better during the Scavenger Hunt Challenge.

Trial III Results					
Object Detection			Audio Classification		
Timestamp from Start (ms)	Prediction	Actual	Timestamp from Start (ms)	Prediction	Actual
40,973	None	Eyeglasses	14,631	Dog Bark	Dog Bark
87,073	Wine Glass	Wine Glass	33,113	Car Horn	Car Horn
157,753	Backpack	Backpack	59,096	Street Music	Street Music
164,923	End at Orange Cone		78,501	Children Playing	Gun Shot
			102,080	Drilling	Siren

**Table 10: Trial III Results**

Furthermore, we note from the timestamps that compared to Trials I and III, Trial II completes its audio classifications and object detections the fastest. As far as audio classification, this demonstrates that Trial II’s edge computing-optimized audio classification model outperforms Trial III’s ResNet model in terms of efficiency, particularly considering Trial II’s audio

model includes an additional 0.5 second delay for filtering. It is more difficult to compare the efficiency of Trial II and Trial III's object detection models from the timestamps because these logs are a function not only of inference time but also of the time that it takes the robot itself to navigate the robotics *environment*. Nevertheless, it is suggestive that Trial II's object detection log consistently outpaces Trial III's by around 17,000 milliseconds.

## **Summary and Conclusions**

Our three approaches to implementing object detection and audio classification for robotics applications on the Raspberry Pi yield varying results. We summarize our finding as follows:

- High-efficiency models are critical for real-time decision making on low-power devices. Recent advances in mobile-optimized architectures strike a balance between high-accuracy and high-efficiency.
- Integer quantization of models additionally increases efficiency with minimal accuracy loss, but not all high-performance deep learning architectures are quantizable using TensorFlow Lite.
- A critical element of audio classification is addressing environmental noise. From our limited trials, real-time noise filtering proves to be a promising approach as compared to training the model on augmented, noisy data. Furthermore, deep learning approaches to audio classification out-perform probabilistic approaches such as HMMs when tested on validation and in real-time for robotics applications, though they do not do so substantially, particularly given the additional compute power required by deep learning models on inference. That said, we make the caveat that part of the difference in performance between these approaches during the Scavenger Hunt Challenge may be due to the difference in microphones employed by the robots.
- Different multithreading schemes yield varying results. We see a notable difference in the amount of time it takes the robot to compete the Scavenger Hunt Challenge between Trial I, which employs a robotics application with five total threads, and Trial II and III, both of which employ a robotics application with only three threads. This is in addition to the

fact that while Trial I and Trial II use an accelerator for inference (NCS in the former case and Coral TPU in the latter), Trial III does not rely on an accelerator.

One key limitation of this study is that we only performed one live Scavenger Hunt Challenge for each of the three Trials. Given the often-tenuous conditions of the robotics *environment*, including the microphones' sensitivities to varying noise conditions and the cameras' sensitivities to varying light conditions, it would be useful to perform multiple tests of each Trial and study the variance of the performance of the three Trials. Moreover, by using two different types of microphones, we limited our ability to effectively compare the accuracy of our audio classification models. Future research should ensure that all sensor equipment (e.g. cameras, microphones, distances sensors) is consistent across Trials.

Across all three Trials, our audio classification models had a more difficult time classifying shorter sound samples such as the Gun Shot. As such, future studies may consider training audio classifications models – be they neural networks or HMMs – using sample lengths that match the average length of the shortest audio class. In the case of the *UrbanSounds8K*, this would mean that four-second sound samples would need to be divided into multiple one or two-second sound samples to match the average length of the Gun Shot sound sample.

Next, because each of our deep learning models for audio classification only unfroze a minimal number of layers – if any – when employing transfer learning, future studies may wish to experiment with unfreezing more layers.

Finally, we discuss how one of the greatest challenges of HMMs is the requirement that the user decide *a priori* the number of latent variables. As a result, future research may consider exploring the use of a variant of a Hierarchical Dirichlet Process HMM (HDP-HMM) as proposed by Fox (2009) in order to determine the appropriate number of hidden states

conditioned on the data via Gibbs sampling or a related method. Such HDP-HMMs may rival or even out-perform deep learning approaches to audio classification.

In the end, with the growing computational power of mobile computing devices such as the Raspberry Pi in addition to the availability of small USB accelerators such as the ones employed in this research, we see ample opportunity for the growth of cheap and effective intelligent devices going forward.

## References

- Asan, U. & Ercan, S. (2011). An Introduction to Self-Organizing Maps. In Cengiz Kahraman (Eds.), *Computational Intelligence Systems in Industrial Engineering with Recent Theory and Applications* (pp. 299-319). Atlantis Press.
- Audacity Team. (2015, March 30). *How Audacity Noise Reduction Works*. Audacity. Retrieved from [https://wiki.audacityteam.org/wiki/How\\_Audacity\\_Noise\\_Reduction\\_Works](https://wiki.audacityteam.org/wiki/How_Audacity_Noise_Reduction_Works)
- Boashash, B. (2016). *Time-Frequency Signal Analysis and Processing: A Comprehensive Reference*. Elsevier.
- Bochkovskiy, A., Wang, C., & Liao, H. (2020). *YOLOv4: Optimal Speed and Accuracy of Object Detection*. Cornell University. <https://arxiv.org/pdf/2004.10934.pdf>
- Bradski, G. & Kaehler, A. (2008). *Learning OpenCV*. O'Reilly Media, Inc.
- Dalal, N. & Triggs, B. 2005. Histograms of oriented gradients for human detection. *Proceedings of the IEEE Conference on Computer Vision and Pattern Recognition*, 886-893. <https://ieeexplore.ieee.org/document/1467360>.
- Davis, S. & Mermelstein, P. (1980). Comparison of parametric representations for monosyllabic word recognition in continuously spoken sentences. *IEEE Transactions on Acoustics, Speech, and Signal Processing*, 28(4): 357-366.
- Dennis, A. K. (2015). *Raspberry Pi Home Automation with Arudino* (2nd ed.). Packt Publishing.
- Felzenszwalb, P. F., Girshick, R. B., McAllester, D., & Ramanan, D. (2010). Object detection with discriminatively trained part-based models. *IEEE Transactions on Pattern Analysis and Machine Intelligence*, 32(9): 1627-1645, 2010.
- Gales, M. & Young, S. (2008). The Application of Hidden Markov Models in Speech Recognition. *Foundations and Trends in Signal Processing*. 1(3), 195-304.

- Gerón, A. (2017). *Hands on Machine Learning with Scikit-Learn and TensorFlow*. O'Reilly Media, Inc.
- Goodfellow, I., Bengio, Y., & Courville, A. (2016). *Deep Learning*. MIT Press.
- Gu, J., et. al. (2018). Recent advances in convolutional neural networks. *Pattern Recognition*. 77, 354–377.
- He, K., Zhang, X., Ren, S., & Sun, J. (2016). Deep Residual Learning for Image Recognition. *IEEE Conference on Computer Vision and Pattern Recognition*.
- Hersey, S., et al. (2017). *CNN Architectures for Large-Scale Audio Classification*. Cornell University. <https://arxiv.org/pdf/1609.09430.pdf>
- Howard, A. G., et al. (2017). *MobileNets: Efficient Convolutional Neural Networks for Mobile Vision Applications*. Cornell University. <https://arxiv.org/pdf/1704.04861.pdf>
- Hui, J. (2018, March 28). What do we learn from single shot object detectors (SSD, YOLOv3), FPN & focal loss (RetinaNet)? Retrieved from medium.com
- Kathuria, A. (2018). What's New in Yolov3. Retrieved from  
<https://towardsdatascience.com/yolo-v3-object-detection-53fb7d3bfe6b>
- Kohonen, T. (2001). *Self-Organizing Maps* (3rd ed.). Springer-Verlag.
- Lin, T. Y., Maire, M., Belongie., S. et. al. (2015). *Microsoft COCO: Common Objects in Context*. Cornell University. <https://arxiv.org/pdf/1405.0312.pdf>
- Liu, R, et al. (2020, March 16). Higher accuracy on vision models with EfficientNet-Lite. Retrieved from <https://blog.tensorflow.org/2020/03/higher-accuracy-on-vision-models-with-efficientnet-lite.html>
- Liu, Wei et al. (2016). “SSD: Single Shot MultiBox Detector.” Lecture Notes in Computer Science (2016): 21–37. Crossref. Web.

Mordor Intelligence. (2019). Robotics Market Size, Growth, Analysis: Growth, Trends, and Forecast (2019 - 2024). Retrieved from <https://www.mordorintelligence.com/industry-reports/robotics-market>.

Redmon, J., Divvala, S., Girshick, R., & Farhadi, A. (2015). *You Only Look Once: Unified, Real-Time Object Detection*. Cornell University. <https://arxiv.org/pdf/1506.02640.pdf>

Redmon, J. & Farhadi, A. (2018). YOLOv3: An Incremental Improvement. Retrieved from <https://pjreddie.com/media/files/papers/YOLOv3.pdf>

Rosebrock, A. (2018). Real Time Object Detection on the Raspberry Pi with the Movidius NCS. Retrieved from <https://www.pyimagesearch.com/2018/02/19/real-time-object-detection-on-the-raspberry-pi-with-the-movidius-ncs/>

Sainbury, T. (2018, July 7). Noise reduction using spectral gating in python. Retrieved from <https://timsainburg.com/noise-reduction-python.html>

Salamon, J., Jacoby, C., & Bello, J.P. (2014). A Dataset and Taxonomy for Urban Sound Research. *Proceedings of the 22nd ACM international conference on Multimedia*, 1041-1044. <https://dl.acm.org/doi/10.1145/2647868.2655045>.

Sandler, M., Howard, A., et al. (2019). *MobileNetV2: Inverted Residuals and Linear Bottlenecks*. Cornell University. <https://arxiv.org/pdf/1801.04381.pdf>

Smith, L. (2017). *Cyclical Learning Rates for Training Neural Networks*. Cornell University. <https://arxiv.org/pdf/1506.01186.pdf>

Tan, M & Le, V. Q. (2019). *EfficientNet: Rethinking Model Scaling for Convolutional Neural Networks*. Cornell University. <https://arxiv.org/pdf/1905.11946.pdf>

Veit, A., Wilber, M., & Belongie, S. (2016). *Residual Networks Behave Like Ensembles of Relatively Shallow Networks*. Cornell University. <https://arxiv.org/pdf/1605.06431.pdf>

Wang, C. (2018, August 13). A Basic Introduction to Separable Convolutions. Retrieved from  
towardsdatascience.com